

## Material Characterization and Continuum Modeling of Poly (Methyl Methacrylate) (PMMA) above the Glass Transition

Arindam Ghatak, Rebecca B. Dupaix \*

*Department of Mechanical Engineering, The Ohio State University, Columbus, OH 43210*

---

### Abstract

Uniaxial compression tests were conducted on poly (methyl methacrylate) (PMMA) over a wide range of strain rates and temperatures in and above the glass transition (from 102°C to 130°C). PMMA exhibits different behavior close to the glass transition (below 115°C) as compared to temperatures farther above the glass transition. In the temperature range just above the glass transition, a clear yield point and strain hardening at higher strains is observed. At temperatures farther above the glass transition, PMMA shows more fluid-like behavior, with no clear yield point or strain hardening at high strains. This change in behavior with temperature poses difficulties in using some of the existing constitutive models, as illustrated by the use of two different models, namely, the Dupaix-Boyce model and the Doi-Edwards model. The data obtained is used to calibrate the two models in order to predict the behavior of PMMA across this industrially significant range of processing temperatures for hot embossing applications.

*Keywords:* uniaxial compression, constitutive model, PMMA, glass transition

---

### 1. Introduction

Poly (methyl methacrylate) (PMMA) is a thermoplastic used in applications ranging from microelectromechanical systems (MEMS), to micro-optics and medical devices. In these applications, it is often necessary to create micro-scale features on the polymer surface using techniques such as hot embossing. Hot embossing can produce micron-scale features and below in thermoplastics such as PMMA (Sotomayor Torres et al., 2003). The hot-emboss process involves localized surface deformation using a die at temperatures above the material's glass transition. Before the die is withdrawn from the material, the polymeric material is cooled below the glass transition temperature in order to "freeze" the material into its final embossed shape. However, the material does experience some spring-back from its embossed position after die removal, even with substantial cooling. Therefore, it is important to understand the relationships between spring-back, rate of loading, and processing temperatures in order to predict and optimize embossing processes while retaining quality features.

In order to better understand the behavior of PMMA, uniaxial compression tests were conducted over a range of strain rates and temperatures. The stress-strain behavior obtained from the tests was then fit to the Dupaix-Boyce and Doi-Edwards models. A significant change in the behavior of PMMA was observed as it was heated to progressively higher temperatures. Beginning at temperatures around 115-120°C, PMMA begins to exhibit more fluid-like behavior. There is significant softening of the material at higher temperatures with no clear yield point and a loss of strain hardening. While the Dupaix-Boyce model successfully captures the behavior of PMMA between 102 and 115°C, the fluids-based Doi-Edwards model better captures its behavior between 120 and 130°C.

### 2. Background

Previous experimental work on PMMA near the glass transition has been conducted by Palm et al. (2006), G'Sell and Souahi (1997), and Dooling et al. (2002). Recent work by Palm et al. (2006) used the Dupaix-Boyce model (Dupaix and Boyce, 2007) to capture the behavior of PMMA at temperatures above the glass transition ( $\theta_g$ ), though the temperature range explored in that work was limited to temperatures up to  $\theta_g+13^\circ\text{C}$  (115°C). Another model by Dooling et al. (2002) also attempts to capture this temperature range with good results over the temperature range 114 to 190°C (all above  $\theta_g$ ), and includes rate dependence. A very recent model by Richeton et al. (2007) is able to capture the behavior of PMMA over a wide range of temperatures and rates, though it requires a large number of fitting constants and may have numerical problems in simulating cooling effects, as will be discussed later.

Fluids-based approaches to modeling polymer mechanical behavior have also been used at temperatures approaching the glass transition from above (Hirai et al., 2003; Juang et al., 2002a, 2002b; Rowland, 2005a, 2005b;

---

\*Email: dupaix.1@osu.edu

Scheer, 2005a, 2005b). These models have been used in hot embossing simulations, with a viscosity-temperature relationship as the input material model. However, these models often fall short in capturing the behavior closer to  $\theta_g$  and are especially questionable below  $\theta_g$ . We seek a model that can capture the full range of behavior across the glass transition, but for illustrative purposes show the ability of one fluids-based model by Doi and Edwards (Doi, 1980; Doi and Edwards, 1978, 1986) to capture the behavior at temperatures more than 15 degrees above  $\theta_g$ .

### 3. Experimental Details

Cylindrical test specimens of 10 mm average diameter and 7.78 mm average height were used for uniaxial compression testing. The specimens were machined from sheet stock supplied by Plaskolite, Inc. (molecular weight = 140,000) and were stored in a desiccant chamber prior to testing. The experiments were conducted using an Instron 5869 electromechanical load frame with a 50 kN load cell and an Instron 5800 controller run by Instron BlueHill software. Friction was minimized by placing Teflon sheets and WD-40 lubricant between the specimen and the compression platens, with care taken to avoid contact between the lubricant and the test specimens. The test specimens were heated to test temperatures ranging from 102°C to 130°C and were allowed to equilibrate for 20 minutes prior to testing. Strain rates ranged from -0.05/min to -6.0/min and specimens were compressed to a final true strain of -1.5 to -2.0.

### 4. Experimental Results

Figures 1 through 6 show how the stress-strain behavior depends on strain rate. Plots show true stress versus true strain at each temperature. As can be seen in these figures, the material behavior stiffens with an increase in strain rate. Furthermore, the material strain hardens at temperatures near the glass transition temperature (Figures 1-3). The amount of strain hardening begins to decrease for temperatures between 115°C and 120°C (Figures 3 and 4) and at temperatures above 120°C, strain hardening is completely absent (Figures 5 and 6). This behavior is also noticeable at 115°C and 120°C for tests at slower strain rates. The yield point in all of these cases is not readily distinguishable. The steep linear elastic portion of the stress-strain curve evident at lower temperatures gives way to much more compliant curves at and above 115°C, coinciding with considerable softening of the material at 115°C and above.

Figures 7 and 8 show temperature dependence through true stress-true strain plots over a range of temperatures at strain rates of -1.0/min and -3.0/min respectively. At higher temperatures, the polymer molecules can more easily move past one another due to increased mobility. Therefore, the stress values are much lower at higher temperatures, as illustrated in these figures. The stress-strain curves at 102°C, 107°C and 110°C show significantly higher stresses and more strain-hardening compared to the higher temperatures. There is a distinct yield followed by a small amount of strain softening evident at 102°C and 107°C at these higher strain rates. The reason for the softening at temperatures close to  $\theta_g$  (especially at high strain rates) is the prior thermal history and aging of the sample. The observations above make it clear that different mechanisms are at work at temperatures below and above 115°C. The region between 115°C and 120°C can be seen as a transition period, wherein we see “fluid-like” stress-strain characteristics emerge, though a small amount of strain hardening still persists at higher strain levels.

Overall, the experimental results are consistent with other results in the literature. In particular, strong rate and temperature dependence is observed and this data clearly shows a transition in behavior from temperatures close to but above  $\theta_g$  to temperatures more than 15 degrees above  $\theta_g$ .

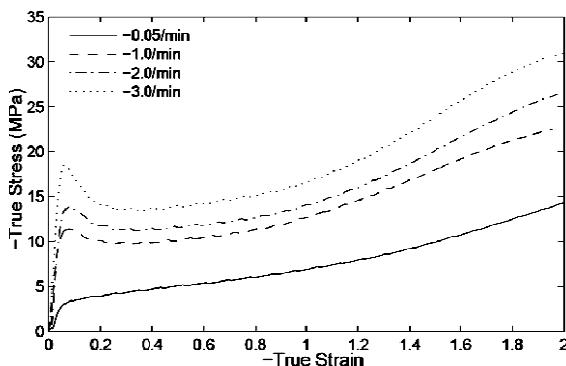


Figure 1: Uniaxial compression experimental data at 102°C.

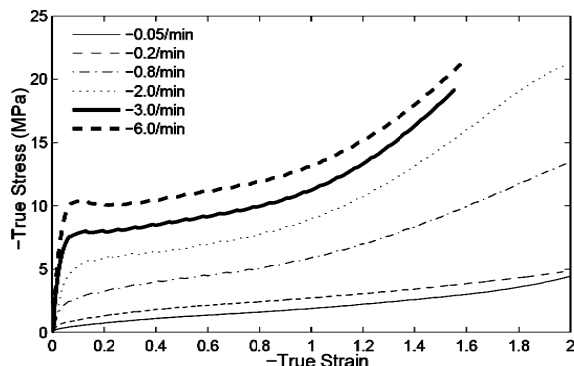


Figure 2: Uniaxial compression experimental data at 110°C.

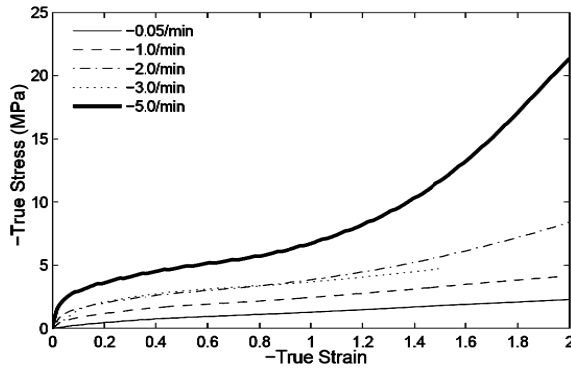


Figure 3: Uniaxial compression experimental data at 115°C.

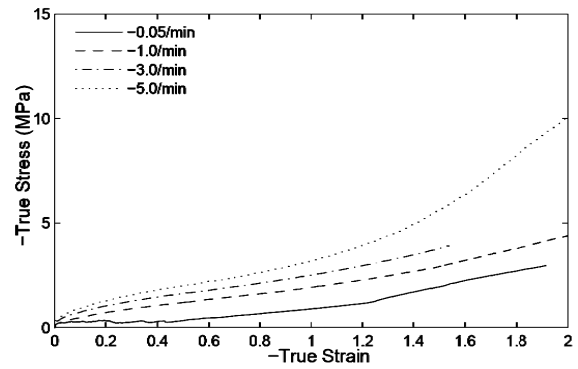


Figure 4: Uniaxial compression experimental data at 120°C.

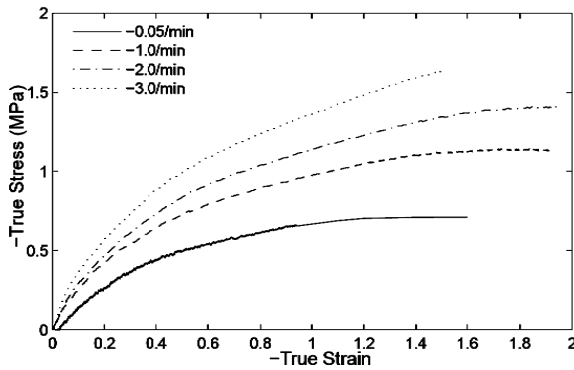


Figure 5: Uniaxial compression experimental data at 125°C.

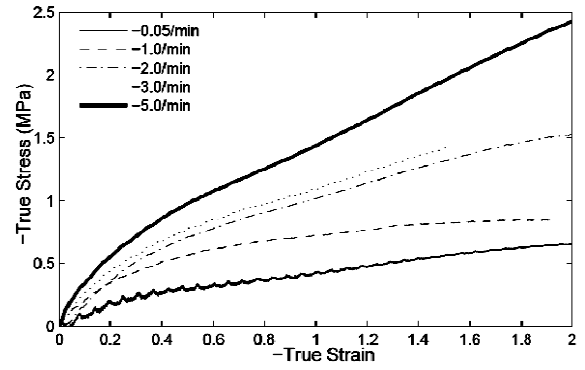


Figure 6: Uniaxial compression experimental data at 130°C.

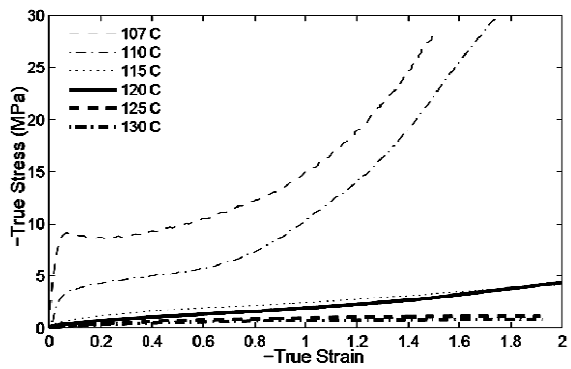


Figure 7: Uniaxial compression experimental data at a strain rate of -1.0/min

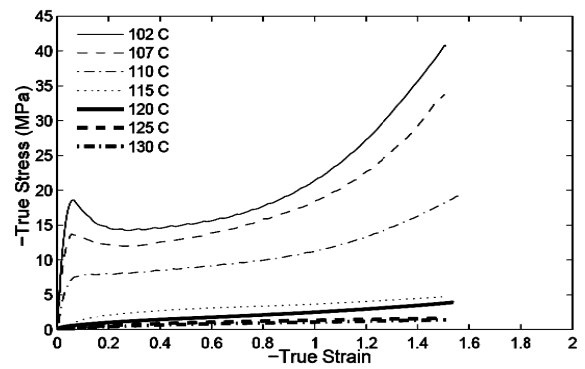


Figure 8: Uniaxial compression experimental data at a strain rate of -3.0/min

## 5. Constitutive Modeling

In this section, we investigate the ability of two models to capture the observed experimental behavior of PMMA.

### 5.1. Dupaix-Boyce Model

The Dupaix-Boyce model has previously been used to capture the mechanical behavior of PMMA up to temperatures of  $\theta_g + 13^\circ\text{C}$  (Palm et al., 2006) and here we attempt to extend its application to even higher temperatures. The details of the model can be found in earlier work (Dupaix and Boyce, 2007), but a brief summary is given here.

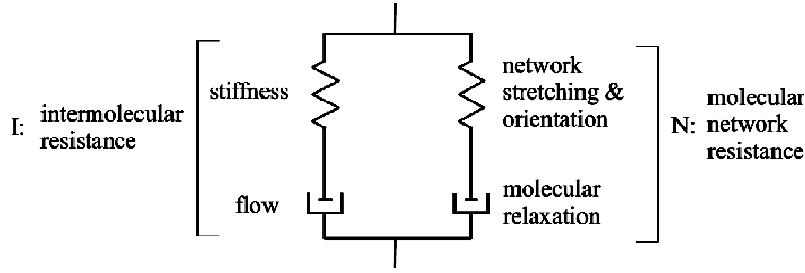


Figure 9: Schematic of the Dupaix-Boyce constitutive model

A schematic of the constitutive model is shown in Figure 9, where the model is interpreted with two resistances (intermolecular: I and network: N). The parallel nature of the model implies that the total stress is equal to the sum of the Cauchy stress in each branch:  $\mathbf{T} = \mathbf{T}_I + \mathbf{T}_N$  and the deformation gradient in each branch is equal to the total deformation gradient:  $\mathbf{F}_I = \mathbf{F}_N = \mathbf{F}$ . Each deformation gradient is decomposed into elastic and plastic parts multiplicatively and the plastic spin in the elastically loaded configuration is prescribed to be equal to zero, to make the formulation unique. A constitutive model for each spring is needed to relate the stress to the elastic deformation gradient. Constitutive models for each damper relate the plastic strain rate to the shear stress, which is then used to determine the rate of plastic straining.

The constitutive equations are as follows. The elastic part of (I) is taken to be linearly elastic:

$$\mathbf{T}_I = \frac{1}{J_I} C^e [\ln \mathbf{V}_I^e] \quad (1)$$

where  $J_I = \det \mathbf{F}_I^e$  is the volume change,  $\frac{1}{J} [\ln \mathbf{V}_I^e]$  is the Hencky strain (Anand, 1979),  $C^e$  is the fourth order tensor of elastic constants, and the superscript  $e$  denotes the elastic part of the deformation gradient.

The plastic part of (I) is assumed to follow a thermally activated process:

$$\dot{\gamma}_I^p = \dot{\gamma}_{0I} \exp \left[ -\frac{\Delta G_I (1 - \tau_I / s_I)}{k \theta} \right] \quad (2)$$

where  $\Delta G_I$  is the activation energy of the material which must be overcome before flow can begin,  $\dot{\gamma}_{0I}$  is a pre-exponential factor,  $s_I$  is the shear resistance, taken to be 0.15 times the shear modulus,  $k$  is Boltzmann's constant,  $\theta$  is the absolute temperature of the material, and  $\tau_I$  is the magnitude of the deviatoric stress (Dupaix and Boyce, 2007).

The shear modulus strongly depends on temperature and is captured through:

$$\mu = \frac{1}{2}(\mu_g + \mu_r) - \frac{1}{2}(\mu_g - \mu_r) \tanh \left( \frac{5}{\Delta \theta} (\theta - \theta_g) \right) + X_g (\theta - \theta_g) \quad (3)$$

where  $\mu_g$  represents the modulus in the glassy region,  $\mu_r$  represents the modulus in the rubbery region,  $\Delta \theta$  is the temperature range across which the glass transition occurs, and  $X_g$  is the slope (of  $\mu$  versus  $\theta$ ) outside the glass transition regime.  $\theta_g$  is the glass transition temperature of the material. Since the modulus ( $\mu$ ) in the glass transition region is also strain-rate dependent, this is taken into account by shifting the glass transition temperature with strain rate as:

$$\theta_g = \begin{cases} \theta_g^* & : \dot{\gamma}_I^p < \dot{\gamma}_{ref} \\ \xi \log_{10} \left( \frac{\dot{\gamma}_I^p}{\dot{\gamma}_{ref}} \right) + \theta_g^* & : \dot{\gamma}_I^p \geq \dot{\gamma}_{ref} \end{cases} \quad (4)$$

$\theta_g^*$  is the reference glass transition temperature taken to be  $104^\circ\text{C}$ ,  $\xi$  is a material constant, and  $\dot{\gamma}_{ref}$  is the reference strain rate, equal to .00173/sec. The bulk modulus is also taken to be temperature dependent, following a similar fashion to equation (3):

$$B = \frac{1}{2}(B_g + B_r) - \frac{1}{2}(B_g - B_r) \tanh\left(\frac{5}{\Delta\theta}(\theta - \theta_g)\right) \quad (5)$$

Resistance  $N$ : molecular network interactions

Resistance  $N$  consists of a highly non-linear spring and a dashpot. While the spring captures the strain-stiffening effects in the polymer, the dashpot represents the molecular relaxation at higher temperatures or lower strain rates. The elastic spring in ( $N$ ) makes use of the Arruda-Boyce 8-chain model:

$$\mathbf{T}_N = \frac{1}{J_N} \frac{\nu k\theta}{3} \frac{\sqrt{N}}{\bar{\lambda}_N} L^{-1}\left(\frac{\bar{\lambda}_N}{\sqrt{N}}\right) \left[ \bar{\mathbf{B}}_N^e - (\bar{\lambda}_N)^2 \mathbf{I} \right] \quad (6)$$

where  $N$  is the number of rigid links between entanglements, and  $\nu$  is the chain density. These are the only two material constants in this equation.  $L^{-1}$  is the inverse Langevin function defined as  $L(\beta) = \coth(\beta) - (1/\beta)$ . The effective chain stretch  $\bar{\lambda}_N$  is given by the root mean square of the distortional applied stretch:

$$\bar{\lambda}_N = \left[ \frac{1}{3} \text{tr}(\bar{\mathbf{B}}_N^e) \right]^{1/2} \quad (7)$$

$$\bar{\mathbf{B}}_N^e = \bar{\mathbf{F}}_N^e (\bar{\mathbf{F}}_N^e)^T, \quad \bar{\mathbf{F}}_N^e = (J_N)^{-1/3} \mathbf{F}_N^e, \quad J_N = \det \mathbf{F}_N^e$$

This model has previously been given temperature dependence, through the constants  $\nu$  and  $N$  (Arruda et al. 1995). However, this can cause numerical problems in simulations involving cooling. The argument inside the inverse Langevin function  $\left(\frac{\bar{\lambda}_N}{\sqrt{N}}\right)$  must always be less than one. If  $N$  is prescribed to increase with temperature, as is done in the Richeton et al. (2007) model, and a simulation is performed at an elevated temperature, then a relatively large value of  $\bar{\lambda}_N$  may be achieved. Now, as the material cools,  $N$  will decrease, possibly to the point that  $\sqrt{N}$  becomes smaller than the current value of  $\bar{\lambda}_N$  and causing a numerical singularity. To avoid this, we interpret the molecular network as being independent of temperature. Instead, temperature is viewed as facilitating reptation, through the molecular relaxation dashpot. The rate of molecular relaxation for resistance  $N$  is given by:

$$\dot{\gamma}_N^p = C \left( \frac{\alpha / \alpha_c - 1}{\alpha_0 / \alpha_c - 1} \right) \left( \frac{\alpha}{\alpha_c} \frac{\tau_N}{\nu k\theta} \right)^{1/n} \quad (8)$$

where  $n$  is a power-law exponent,  $\alpha$  is a measure of the orientation of the polymer chains with initial value  $\alpha_0$ .  $\alpha_c$  is a cutoff value, beyond which molecular relaxation ceases.  $\alpha$  is calculated as:

$$\alpha = \frac{\pi}{2} - \cos^{-1} \left( \frac{\min(\lambda_1, \lambda_2, \lambda_3)}{\sqrt{\lambda_1^2 + \lambda_2^2 + \lambda_3^2}} \right) \quad (9)$$

where  $\lambda_i$  are the principal stretches. The parameter  $C$  is temperature dependent and is given by:

$$C = D \exp \left\{ -\frac{Q}{R\theta} \right\} \quad (10)$$

where  $D$  and  $Q/R$  are material parameters.

There are a total of 15 parameters used in this model, given in Table 1. The two constants that are perhaps the most physically intuitive are the glassy and rubbery modulus. These are intended to represent the initial elastic stiffness of the material below and above the glass transition. The constants were obtained from data fit close to the glass transition temperature, so the ‘‘glassy modulus’’ used here is somewhat lower than would be expected for PMMA at room temperature, because it was obtained just a few degrees below the glass transition. The rubbery modulus may seem a bit high for the very compliant stress-strain curves seen above the glass transition, however, this constant is determined from the very early part of the stress-strain curve before any yielding or flow occurs. Since flow occurs at very low stress levels above the glass transition, the initial elastic behavior has a fairly small effect on the overall stress-strain curve above the glass transition.

Table 1: Material constants for the Dupaix-Boyce model

	Material Property	Symbol	Value
Initial Elastic Behavior	Glassy Modulus	$\mu_g$	325 MPa
	Rubbery Modulus	$\mu_r$	50 MPa
	Temperature Shift	$\Delta\theta$	30 K
	Transition Slope	$X_g$	-3 KPa/K
	Rate Shift Factor	$\xi$	3 K
	Glassy Bulk Modulus	$B_g$	1.0 GPa
	Rubbery Bulk Modulus	$B_r$	2.25 GPa
Flow Stress	Pre-exponential Factor	$\dot{\gamma}_{0I}$	$7.5 \times 10^{13}$ 1/s
	Activation Energy	$\Delta G$	$2.12 \times 10^{-19}$ J
Resistance Elasticity	Rubbery Orientation Modulus	$\nu k\theta$	8.0 MPa
	Entanglement Density	$N$	500
Molecular Relaxation	Temperature Coefficient	$D$	$1.7 \times 10^4$ 1/s
	Second Temperature Parameter	$Q/R$	$1.42 \times 10^7$ K
	Power-law Exponent	$1/n$	6.67
	Cutoff Orientation	$\alpha_c$	0.0012

### Modeling Results

Figures 10 and 11 show the experimental and simulated stress-strain curves for PMMA at 102°C and 110°C at strain rates ranging from -0.05/min to -6.0/min. As can be seen, the model predictions are in good agreement with the test results. However, as figure 12 shows, the model overpredicts the stress values at 115°C. The model overpredicts both the initial modulus and the amount of strain hardening. At even warmer temperatures, as the material softens further, this model is completely unable to capture the stress-strain behavior. It both overpredicts the initial modulus and yield stress, as well as predicts strain hardening that is not observed in experiments at temperatures more than 15 degrees above  $\theta_g$ . In the next section, we discuss the Doi-Edwards model in an attempt to capture this behavior at temperatures more than 15 degrees above  $\theta_g$ .

### 5.2 Doi-Edwards Model

The Doi-Edwards model was developed to capture polymer chain reptation and is a Non-Newtonian fluid model. This approach is used to illustrate the potential of fluids-based modeling at temperatures more than 15 degrees above  $\theta_g$ . In this approach, the phenomenon of stress relaxation is interpreted as a reduction in material modulus over time. This is in contrast to the glass-rubber model just presented, which models stress relaxation as a transfer of deformation from elastic to plastic over time, with unchanged material properties.

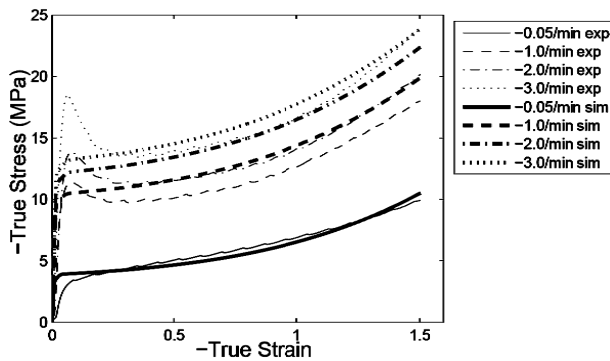


Figure 10: Experimental and simulation results for uniaxial compression tests at the glass transition temperature, 102°C.

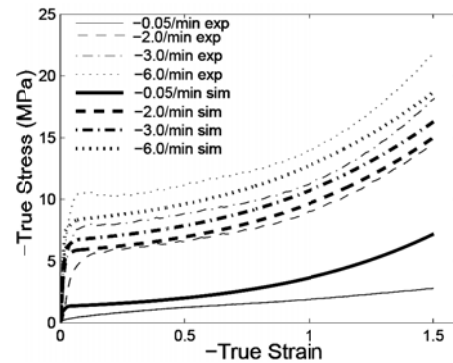


Figure 11: Experimental and simulation results for uniaxial compression tests at 110°C

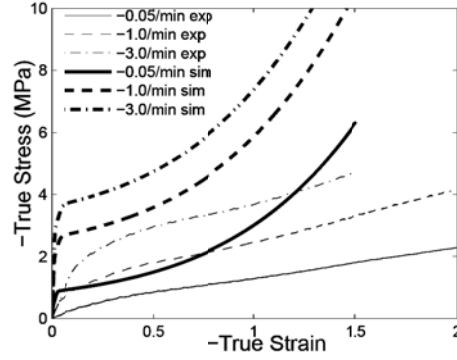


Figure 12: Experimental and simulation results for uniaxial compression tests at 115°C.

The original model development, as contained in (Doi, 1980) is cast in a form to predict stress-strain behavior in uniaxial compression. Detailed derivations of these equations can be found in Dupaix (2003). The components of the stress tensor as a function of time are taken to be

$$\sigma_{\alpha\beta}(t) = G_0 \int_{-\infty}^t dt' \mu'(t-t') Q_{\alpha\beta}[\mathbf{F}(t,t')] \quad (11)$$

where the relaxation modulus  $\mu'$  is given by

$$\mu'(t) = \sum_{p \text{ odd}} \frac{8}{p^2 \pi^2 \tau_p} \exp\left(-\frac{t}{\tau_p}\right) \quad (12)$$

$\tau_p$  is a time constant, and  $p$  is a set of integers. We use only  $p = 1$  since it is shown in (Dupaix, 2003) that adding further terms does not significantly change the results while increasing computation time.

The other variables are the deformation gradient  $\mathbf{F}$ , the components of the Cauchy stress tensor  $\sigma_{\alpha\beta}$ , the unit tangent vector to the polymer chain segment  $\mathbf{u}$ , the current time  $t$ , a reference time in the past  $t'$ , Boltzmann's constant  $k$ , and the temperature of the material  $\theta$ .  $Q_{\alpha\beta}$  is given by:

$$Q_{\alpha\beta}(\mathbf{F}) = \left\langle \frac{(\mathbf{F}\mathbf{u})_\alpha (\mathbf{F}\mathbf{u})_\beta}{|\mathbf{F}\mathbf{u}|^2} - \frac{1}{3} \delta_{\alpha\beta} \right\rangle_0 = \int_s \frac{d^2\mathbf{u}}{4\pi} \left\{ \frac{(\mathbf{F}\mathbf{u})_\alpha (\mathbf{F}\mathbf{u})_\beta}{|\mathbf{F}\mathbf{u}|^2} - \frac{1}{3} \delta_{\alpha\beta} \right\} \quad (13)$$

where  $\langle \rangle_0$  indicates a volume average computed as an integral over the surface of a unit sphere. This is effectively an orientation tensor which accounts for the deformation gradient operating on the unit vector along the chain backbone.

### Uniaxial Deformation

Assuming uniaxial deformation in the z-direction and incompressibility of the material, the deformation gradient becomes

$$\mathbf{F} = \begin{bmatrix} \frac{1}{\sqrt{\lambda}} & 0 & 0 \\ 0 & \frac{1}{\sqrt{\lambda}} & 0 \\ 0 & 0 & \lambda \end{bmatrix} \quad (14)$$

where  $\lambda$  is the applied z-direction stretch and the nonzero components of  $Q_{\alpha\beta}$  can be expressed as:

$$Q_{zz} - Q_{xx} = F_3(\lambda) \equiv \left\langle \frac{\lambda^2 u_z^2 - \lambda^{-1} u_x^2}{\lambda^2 u_z^2 + \lambda^{-1} (u_x^2 + u_y^2)} \right\rangle_o \quad (15)$$

This can be evaluated analytically using spherical coordinates for  $\mathbf{u}$  and the stress is given by:

$$\begin{aligned} \sigma_{zz} - \sigma_{xx} &= G_0 \int_{-\infty}^t dt' \mu'(t, t') Q_{zz} - G_0 \int_{-\infty}^t dt' \mu'(t, t') Q_{xx} \\ &= G_0 \sum_{p \text{ odd}} \frac{8}{p^2 \pi^2 \tau_p} \int_{-\infty}^t dt' \exp\left(-\frac{(t-t')}{\tau_p}\right) F_3(\lambda(t, t')) \end{aligned} \quad (16)$$

For loading at a constant strain rate starting at  $t = 0$ ,

$$\lambda(t, t') = \begin{cases} \exp(\dot{\epsilon} t) & : t' < 0 \\ \exp(\dot{\epsilon}(t-t')) & : t' \geq 0 \end{cases} \quad (17)$$

Taking only the  $p=1$  term and simplifying, equation (16) becomes:

$$\sigma_{zz} - \sigma_{xx} = Z F_3(\exp(\dot{\epsilon} t)) \tau_p \exp\left(\frac{-t}{\tau_p}\right) + Z \int_0^t ds \exp\left(\frac{-s}{\tau_p}\right) F_3(\exp(\dot{\epsilon} s)) \quad (18)$$

$$\text{where } Z = G_0 \frac{8}{\pi^2 \tau_p}.$$

The two constants to be determined are  $Z$  and  $\tau_p$ . Temperature dependence is introduced by making  $Z$  and  $\tau_p$  functions of temperature through the following curve-fit expressions:

$$Z = 1.1 \times 10^{-3} \theta^2 - 0.8859\theta + 178.4393 \quad (19)$$

$$\tau_p = 2 \times 10^{-12} \theta^2 - 15.14\theta + 2899.34 \quad (20)$$

where temperature  $\theta$  is in Kelvin.

### Modeling Results

Figures 13-16 show the experimental and simulated (using the Doi-Edwards model) true stress-strain curves from 115 to 130°C at strain rates of -0.05/min, -1.0/min and -3.0/min. The Doi-Edwards model is able to capture the initial slope of the stress-strain curves successfully. However, the fit at higher strains is not as good, especially at temperatures between 115°C and 120°C. The reason for this is that at temperatures around 115°C, there is a small amount of strain hardening taking place, and strain hardening effects are not included in the Doi-Edwards model. At higher temperatures, where strain hardening is absent from the data, the Doi-Edwards model does a much better job. At all temperatures, the Doi-Edwards model can partially capture rate dependence, but its predictive abilities are very poor for the lowest strain rate.

## 6. Discussion and Conclusions

Uniaxial compression tests were conducted over a wide range of temperatures and strain rates on PMMA to verify and improve upon the models described in (Doi, 1980; Doi and Edwards, 1978, 1986; Palm et al., 2006). The experimental results were consistent with previous experimental data in this temperature range (Dooling et al., 2002; G'Sell and Souahi, 1997; Palm et al., 2006). Test results up to about 115°C show material characteristics of typical polymer materials which undergo elastic deformation followed by plastic deformation accompanied by strain hardening, especially at higher strain rates and lower temperatures.

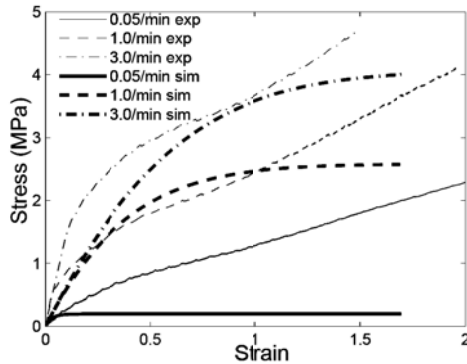


Figure 13: Experimental and simulation results for uniaxial compression tests at 115°C using the Doi-Edwards model.

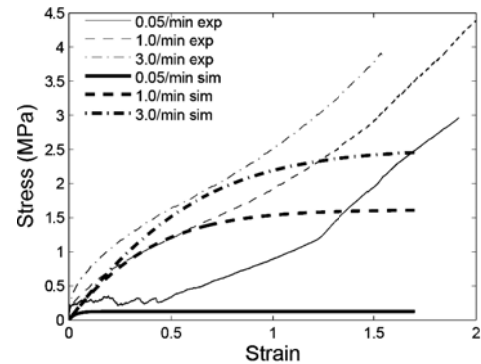


Figure 14: Experimental and simulation results for uniaxial compression tests at 120°C using the Doi-Edwards model.

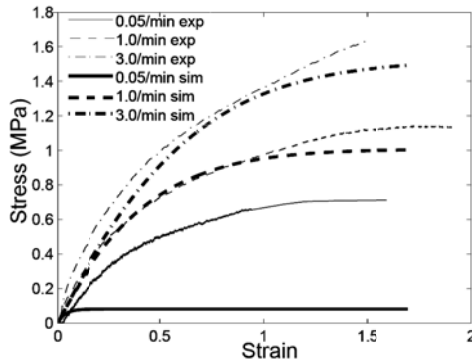


Figure 15: Experimental and simulation results for uniaxial compression tests at 125°C using the Doi-Edwards model.

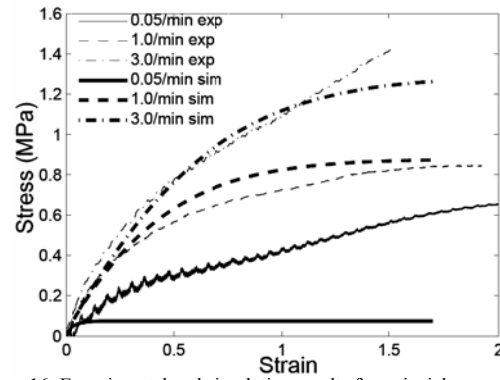


Figure 16: Experimental and simulation results for uniaxial compression tests at 130°C using the Doi-Edwards model.

Test results above 115°C show significantly different behavior, including significant softening of the material, no distinguishable yield point, and a reduction in and ultimate elimination of strain hardening. At higher temperatures around 125°C and 130°C, PMMA behaves like a pseudo-fluid with no strain hardening. The Dupaix-Boyce model works well for capturing lower temperature behavior, but a fluids-based model, such as the Doi-Edwards model, is better for capturing the behavior at temperatures more than 15 degrees above the glass transition temperature. The Doi-Edwards model, in particular, was also shown to have some limitations even in the warmest temperature regime. While the model replicated the test results well at higher temperatures of 125°C and 130°C, it could not capture the observed strain hardening at temperatures closer to the glass transition (115°C and 120°C). Furthermore, although the model successfully predicts stress values at relatively high strain rates, it was not able to effectively capture the behavior of the material at the slowest strain rate.

The Doi-Edwards model in its present state does not incorporate strain hardening at higher strains. Strain hardening models explored in the fluids literature (such as Giesekus, 1982; Ianniruberto and Marrucci, 2001; Wiest, 1989) are one possible direction for improvement. This would be especially important in the transition zone between 115°C and 120°C, which is characterized by material softening due to high temperature but also strain hardening at high strains. More critically, since PMMA behaves differently in the two different temperature ranges, in this work it had to be modeled using two different models. In order to perform 3-D simulations, the two models would have to be seamlessly integrated, a non-trivial task since one model is differential and the other integral in nature. Future work in this area is certainly warranted to try to develop a combined model that can capture this transition from strain hardening-based network-like behavior to molecular relaxation-dominated, fluid-like behavior. The recent model of Richeton, et al. (2007) is clear progress in modeling the large strain behavior over the wide temperature range across the glass transition. However, there are some concerns with how that model would be able to handle non-isothermal situations where the material is cooled while highly stretched. We anticipate that many of the ideas in their paper will be helpful in future modeling development.

Another recent model of Ames, et al. (2009) is also a large step forward in modeling behavior in this complex temperature regime. Their model essentially adds a third branch to the schematic used in the Dupaix-Boyce model and

depending on whether the material is below or above the glass transition, either branch 2 or branch 3 becomes active in the model. The main drawback to using this model in simulations is the need to fit close to 50 material constants, so it seems there is still room for improvement in developing a practical model for hot embossing simulations.

In spite of the limitations shown here for the Dupaix-Boyce model at temperatures more than 15 degrees above the glass transition, even a limited model may be fairly successful in predicting hot embossing outcomes (Cash and Dupaix, 2008). It largely depends on the precise temperature range of interest, the relevant time scales (strain rates), as well as the level of deformation expected in the embossing operation. Regardless of the choice of model, since all of these models were developed from data collected on isothermal experiments, care must be taken when modeling processes involving potentially large temperature changes so as to avoid introducing artifacts into the simulations.

## References

- Anand, L., 1979, On H. Hencky's Approximate Strain Energy Function for Moderate Deformations, *J. Applied Mech.*, **46**, 78-82.
- Ames, N.M., Srivastava, V., Chester, S.A., and Anand, L., 2009, A thermo-mechanically-coupled theory for large-deformations of amorphous polymers. Part II: Applications. *International Journal of Plasticity*, **25**, 1495-1539.
- Arruda, E.M., Boyce, M.C., and Jayachandran, R., 1995, Effects of strain rate, temperature and thermomechanical coupling on the finite strain deformation of glassy polymers, *Mechanics of Materials*, **19**, 193-212.
- Dupaix, R.B. and Cash, W., 2009, Finite Element Modeling of Polymer Hot Embossing: Effects of Temperature on Springback and Residual Stress, *Polymer Engineering and Science*, **39**, 531-543.
- Doi, M., 1980, A constitutive equation derived from the model of Doi and Edwards for concentrated polymer solutions and polymer melts, *Journal of Polymer Science: Polymer Physics Edition*, **18**, 2055-2067.
- Doi, M. and Edwards, S.F., 1978, Dynamics of concentrated polymer systems. Part 3 – the constitutive equation. *Journal of the Chemical Society – Faraday Transactions II*, **74**, 1818-1832.
- Doi, M. and Edwards, S.F., 1986, The theory of polymer dynamics, *Oxford University Press*.\*\*\*\*\*
- Dooling, P.J., Buckley, C.P., Rostami, S., and Zahlan, N., 2002, Hot-drawing of poly(methyl methacrylate) and simulation using a glass-rubber constitutive model, *Polymer*, **43**, 2451-2465.
- Dupaix, R.B., 2003, Temperature and rate dependent finite strain behavior of poly (ethylene terephthalate) and poly (ethylene terephthalate)-glycol above the glass transition temperature, PhD Thesis, MIT, Boston, MA.\*\*\*\*\*
- Dupaix, R.B., Boyce, M.C., 2007, Constitutive modeling of the finite strain behavior of amorphous polymers in and above the glass transition, *Mechanics of Materials*, **39**, 38-52.
- G'Sell, C. and Souahi, A., 1997, Influence of Crosslinking on the Plastic Behavior of Amorphous Polymers at Large Strains, *Journal of Engineering Materials and Technology*, **119**, 223-227.
- Giesekus, H., 1982, A simple constitutive equation for polymer fluids based on the concept of deformation-dependent tensorial mobility, *Journal of Non-Newtonian Fluid Mechanics*, **11**, 69-109.
- Hirai, Y., Yosikawa, T., Takagi, N., Yoshida, S., and Yamamoto, K., 2003, Mechanical Properties of Poly-methyl methacrylate (PMMA) for Nano Imprint Lithography, *Journal of Photopolymer Science and Technology*, **16**, 615-620.
- Ianniruberto, G. and Marrucci, G., 2001, A simple constitutive equation for entangled polymers with chain stretch, *Journal of Rheology*, **45**, 1305-1318.
- Juang, Y.J., Lee, L.J., and Koelling, K.W., 2002a, Hot embossing in microfabrication. Part I: Experimental, *Polymer Engineering and Science*, **42**, 159-165.
- Juang, Y.J., Lee, L.J., and Koelling, K.W., 2002b, Hot embossing in microfabrication. Part II: Rheological characterization and process analysis, *Polymer Engineering and Science*, **42**, 551-566.
- Palm, G., Dupaix, R.B., Castro, J., 2006, Large strain mechanical behavior of poly (methyl methacrylate) (PMMA) near the glass transition temperature, *Journal of Engineering Materials and Technology-Transactions of the ASME*, **128**, 559-563.
- Rowland, H.D., Sun, A.C., Schunk, P.R., and King, W.P., 2005a, Impact of polymer film thickness and cavity size on polymer flow during embossing: Toward process design rules for nanoimprint lithography, *Journal of Micromechanics and Microengineering*, **15**, 2414-2425.
- Rowland, H.D., King, W.P., Sun, A.C., and Schunk, P.R., 2005b, Simulations of nonuniform embossing: the effect of asymmetric neighbor cavities on polymer flow during nanoimprint lithography, *Journal of Vacuum Science and Technology*, **6**, 2958-2962.

- Richeton, J., Ahzi, S., Vecchio, K.S., Jiang, F.C., and Makradi, A., 2007, Modeling and validation of the large deformation inelastic response of amorphous polymers over a wide range of temperatures and strain rates, *International Journal of Solids and Structures*, **44**, 7938-7954.
- Scheer, H.-C., Bogdanski, N., Wissen, M., Konishi, T., and Hirai, Y., 2005a, Polymer time constants during low temperature nanoimprint lithography, *Journal of Vacuum Science and Technology*, **23**, 2963-2966.
- Scheer, H.-C., Bogdanski, N., and Wissen, M., 2005, Issues in nanoimprint processes: the imprint pressure, *Japanese Journal of Applied Physics*, **44**, 5609-5616.
- Sotomayor Torres, C.M., Zankovych, S., Seekamp, J., Kam, A.P., Clavijo Cedeño, C., Hoffmann, T., Ahopelto, J., Reuther, F., Pfeiffer, K., Bleidiessel, G., Gruetzner, G., Maximov, M.V., Heidari, B., 2003, Nanoimprint lithography: an alternative nanofabrication approach. *Materials Science and Engineering*, **23**, 23-31.
- Wiest, J. M., 1989, A differential constitutive equation for polymer melts, *Rheologica Acta*, **28**, 4-12.